ISSN 1061-8309, Russian Journal of Nondestructive Testing, 2018, Vol. 54, No. 6, pp. 443–447. © Pleiades Publishing, Ltd., 2018.
Original Russian Text © S.E. Shipilov, I.S. Tseplyaev, R.N. Satarov, A.I. Eremeev, V.P. Yakubov, I.K. Kurkan, 2018, published in Defektoskopiya, 2018, No. 6, pp. 41–45.

RADIATION NONDESTRUCTIVE TESTING

Subsurface Radiolocation Tomography of Cables under Dual-Polarization Probing

S. E. Shipilov[a, *], I. S. Tseplyaev[a], R. N. Satarov[a], A. I. Eremeev[a], V. P. Yakubov[a], and I. K. Kurkan[b]

[a] *Tomsk State University, Tomsk, 634050 Russia*

[b] *Tomsk Polytechnic University, Tomsk, 634034 Russia*

**e-mail: s.shipilov@gmail.com*

Received July 15, 2015

Abstract—It is proposed to use the tomographic approach to the problem of detecting and imaging concealed utility networks. This approach is based on generating the three-dimensional radio images of the space being explored from the results of measuring its location wave projections in a dual-polarization measurement mode. The problem is solved by focusing radiation first on the “air–dielectric” interface and then inside the dielectric. Experimental data processing results and reconstructed three-dimensional radio tomograms are provided for a “twisted pair” cable and a fiber-optic cable with no metallic inclusions. The results confirm the operability of the approach.

Keywords: radio tomography, ultra-wideband tomography, radiation focusing

DOI: 10.1134/S1061830918060086

INTRODUCTION

One of the tasks in subsurface detection and ranging is to develop efficient approaches to detecting and imaging concealed utility networks. This task is complicated if the detection object is an extended cable buried to a depth of more than 30 cm, in which case the use of metal detectors for revealing it becomes problematic or simply impossible for fiber-optic cables with no metallic inclusions. Subsurface radars can help solving problems of the kind. They are actively used when hunting for hidden archaeological grave sites and searching for concealed utility networks or anti-personnel mines [1, 2]. The complexity of detecting thin extended cables is related to the often-misaligned probing-radiation polarization and cable orientation. As the amplitude of a reflected signal is due to the currents induced on medium inhomogeneities, the orientation of the probing-pulse polarization with regard to the orientation of the object itself plays an important role. Linearly polarized antennas are, as a rule, used for probing in an ultra-wideband frequency range. If the polarization plane does not coincide with the orientation of an extended object (for example, a cable), the reflected-signal amplitude drops and attains its minimum when the cable is orthogonal to the probing-pulse polarization. Therefore, probing with two orthogonal polarizations will ensure a high reflected-signal level whatever the cable orientation is in the subsurface layer.

In order to solve the problem of detecting and imaging concealed utility networks, the authors propose to use the tomographic approach for producing three-dimensional radio images of the examined space from the results of measuring its location wave projections in a dual-polarization measurement mode. When radio-frequency radiation penetrates a medium, one can speak of reconstructing its internal structure based on transmitted or scattered field. This structure is represented by the spatial distribution of the values of dielectric permittivity. Steep permittivity gradients are typical of interfaces between media or of objects immersed in them. Although such problems are far from being simple, a number of efficient solution methods based on the phenomenon of radiation focusing have been developed for them [1–3]. It is important to stress that one should use the phase information contained in the picked-up wave projections of examined objects. It is clear from general considerations that the large-aperture synthesis method should be given preference when processing these projections as it is the most advanced in terms of achieving high spatial resolution. This method already has many varieties, which keep being improved, with the radio wave tomosynthesis being one of them. The latter is based on the principle of radiation focusing and the aperture synthesis technique. The mathematical aspects of this approach were considered in detail by the authors in [2].

The goal of this paper was to practically apply the ultra-wideband (UWB) radio tomography methods previously developed by the authors to the problem of concealed utility networks. Experimental data were gathered using the small-scale UWB radio tomograph developed at the chair of radio physics of Tomsk State University and based on a two-coordinate scanner with dual-polarization probing.

RADIO WAVE TOMOSYNTHESIS IN DUAL-POLARIZATION PROBING

Radio wave tomosynthesis is a generalization of the Fourier synthesis to the case of wave fields. Its core idea is to relate the spatial spectrum of received signal for a certain aperture to the spatial spectrum of sources via a direct proportion.

If the radiation is observed at a point **r** that belongs to a free space and is located at some distance H above the interface between media, its magnitude is linked to the surface field distribution by the simple relation [2, 4]

$$\mathrm{E}(\mathbf{r}) = (2\pi)^{-2}\iint \hat{\mathrm{E}}_s(\boldsymbol{\kappa}_\perp)\exp(i\boldsymbol{\kappa}_\perp\mathbf{r} + i\kappa_z H)d^2\boldsymbol{\kappa}_\perp.$$

Here $\hat{\mathrm{E}}_s(\boldsymbol{\kappa}_\perp)$ denotes a two-dimensional spatial spectrum for the surface distribution of the field $\mathrm{E}(\mathbf{r})$ and

$$\kappa_z = \sqrt{(2k)^2 - \kappa_x^2 - \kappa_y^2} = \sqrt{(2k)^2 - \boldsymbol{\kappa}_\perp^2}.$$

Solving the inverse problem of subsurface tomography of inhomogeneities concealed behind the interface region reduces to calculating the spectrum of the spatial frequencies of received field

$$\hat{\mathrm{E}}(\boldsymbol{\kappa}_\perp) = \iint \mathrm{E}(\mathbf{r})\exp(-i\boldsymbol{\kappa}_\perp\mathbf{r})d^2\boldsymbol{\kappa}_\perp.$$

This spectrum is then recalculated to the plane of the interface region S

$$\hat{\mathrm{E}}_s(\boldsymbol{\kappa}_\perp) = \hat{\mathrm{E}}(\boldsymbol{\kappa}_\perp)\exp(-i\kappa_z H).$$

Focusing the field inside the background medium and determining the spectrum of the spatial frequencies of currents at depth h are implemented as follows:

$$\hat{j}(\boldsymbol{\kappa}_\perp) = -\exp(-i\kappa_z h)2i\kappa_z\,\hat{\mathrm{E}}_s(\boldsymbol{\kappa}_\perp).$$

This is followed by reconstructing an equivalent spatial distribution of the current

$$j(\mathbf{r}) = (2\pi)^{-2}\iint \hat{j}(\boldsymbol{\kappa}_\perp)\exp(-i\boldsymbol{\kappa}_\perp\mathbf{r})d^2\boldsymbol{\kappa}_\perp,$$

which is related to the sought-for permittivity via the expression

$$j(\mathbf{r}) = \frac{k^2}{4\pi|\mathbf{r} - \mathbf{r}_s|}\Delta\varepsilon(\mathbf{r}).$$

The latter operation is tantamount to reconstructing the distribution of inhomogeneities $\Delta\varepsilon(\mathbf{r})$. It should be noted that, in the general case, the derived distribution $\Delta\varepsilon(\mathbf{r})$ is a complex quantity and the envelope of the analytical signal of the original quantity $\Delta\varepsilon_a(\mathbf{r})$ has been used to represent it as a set of layerwise radar images. As a result, the derived distribution is proportional to the jump of the real part of permittivity in the explored volume of space.

As mentioned above, the misalignment between the polarization plane and the orientation of cable-like extended objects reduces the reflected signal amplitude. Two orthogonal probing-signal polarizations need to be used to construct a high-contrast image for an arbitrarily oriented cable. The resulting radio image will then be calculated as the sum of two radio images obtained for two mutually orthogonal polarizations

$$\Delta\varepsilon_a(\mathbf{r}) = \Delta\varepsilon 1_a(\mathbf{r}) + \Delta\varepsilon 2_a(\mathbf{r}).$$

SUBSURFACE RADIO TOMOGRAPHY OF METALLIC AND FIBER-OPTIC CABLES

The operability of the radio wave tomosynthesis was tested by performing the tomography of trial objects placed in a box with river sand occasionally containing inhomogeneities in the form of finely broken stones. The box was 50 cm wide, 120 cm long, and 40 cm tall. Location wave projections were generated with a radio tomograph that included the scanner in the form of a two-coordinate positioning device (Fig. 1), a CABAN R140 vector reflectometer (Fig. 2) that performed step scanning within a prescribed

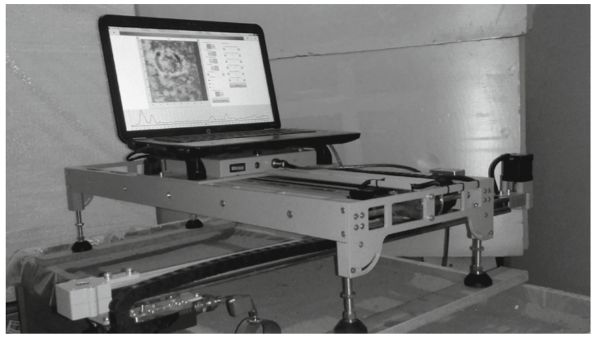

Fig. 1. Radio tomograph diagram.

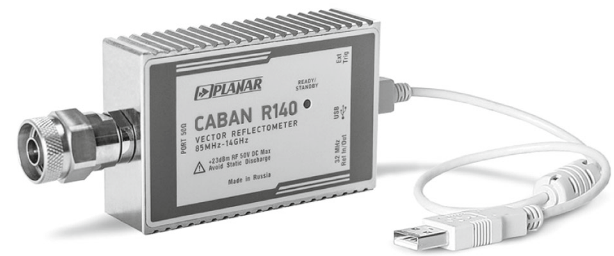

Fig. 2. Vector reflectometer.

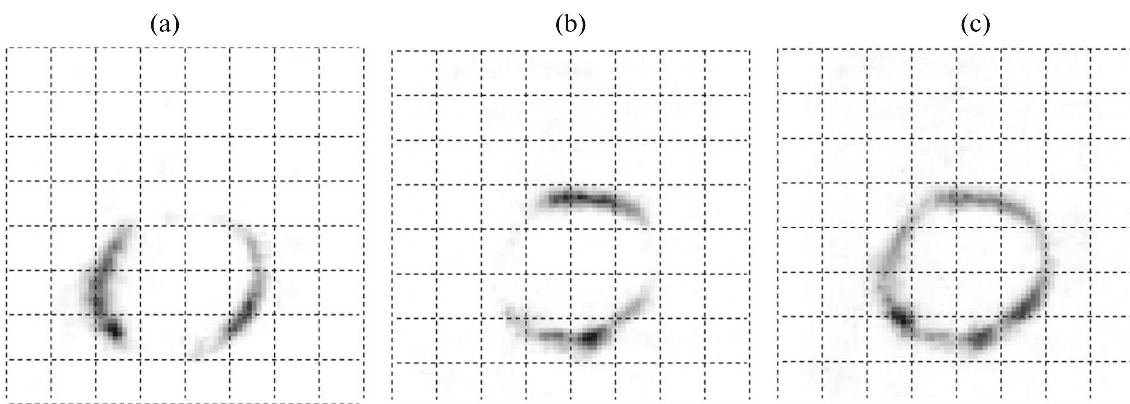

Fig. 3. Radio images of "twisted pair" cable at depth 28 cm.

frequency range from 1 to 10 GHz, a PC, and a linearly polarized transceiving UWB antenna. Scanning was performed using stepper motors, with the scanning time for a 40 × 40 cm area being 5 min. Two orthogonal polarizations were obtained by antenna rotation and repeated scanning of the examined space.

A "twisted pair" cable rolled into a 17-cm-diameter coil and buried in the sand box at a depth of 28 cm was used as the test object. Figure 3 shows the radio images of the cable obtained for each of the two orthogonal probing-radiation polarizations (Figs. 3a and 3b) and their sum (Fig. 3c). Each cell in the pictures is 5 × 5 cm.

Figure 4a represents a three-dimensional radio tomogram of the entire space being examined. Reconstructing the permittivity jump by layers showed, first, "air–sand" interface *1* and, second, some inhomogeneities *2* in the subsurface layer. Further down, one can see coiled cable *3* and a test object in the form of a metal ball *4*, which was initially used to calibrate the tomograph. Even lower, one can trace sandbox bottom *5* and "air–floor" interface *6*. In addition, Fig. 4b depicts the graph of the normed distribution of inhomogeneities over the range, in which the first maximum coincides with the "air–sand" interface

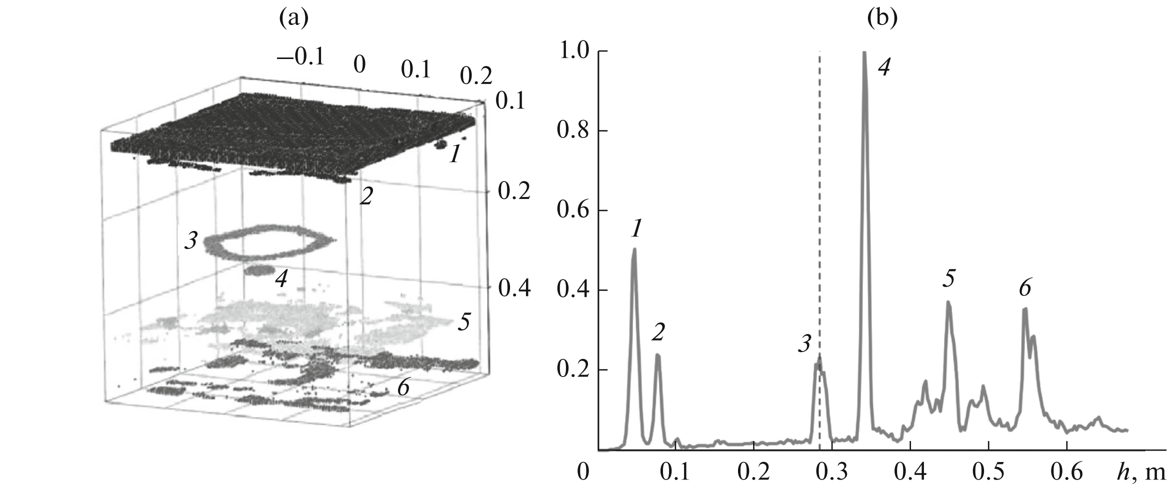

Fig. 4. Three-dimensional radio tomogram of "twisted pair" cable (a) and integral distribution of inhomogeneities over range (b).

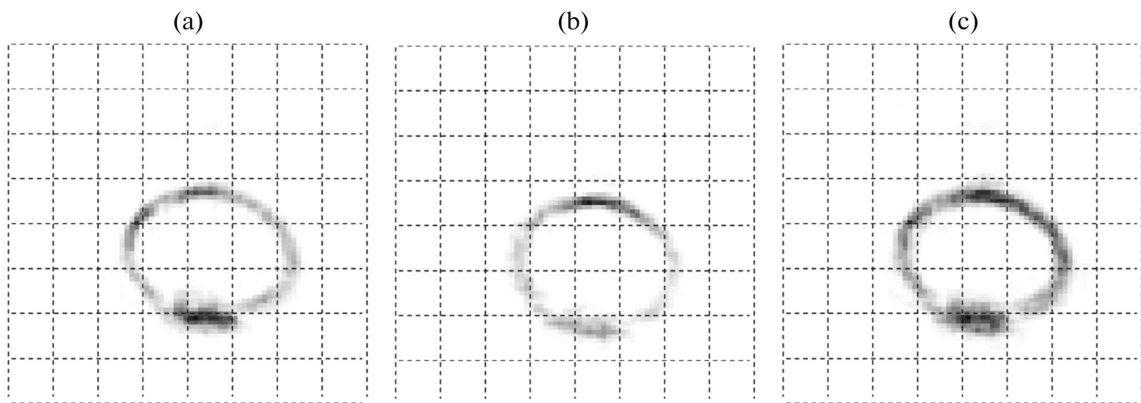

Fig. 5. Radio images of fiber-optic cable at depth 26 cm.

position *1* and the subsequent maxima reflect the depths of the above-described inhomogeneities. The third maximum is at the depth of 28 cm and represents the cable buried in the sand. The availability of the graph of the integral distribution of intensity *I* of inhomogeneities versus the depth allows the operator to navigate easily in three-dimensional radio tomograms and display promptly on screen the image of the layer at a given depth.

Similar measurements were taken for a fiber-optic cable with no metallic inclusions. The permittivity of such objects is close to that of sand, thus disallowing the production of the high-contract images of fiber-optic cables by tomosynthesis. As a rule, when placed in soil such cables are "dressed" into high-strength-plastic tubes for protection against rodents and other harmful actions. In this case, there is an interlayer of air between the cable and tubing, which helps improving the contrast of radio images.

For the purposes of testing, a fiber-optic cable free of metallic inclusions was "dressed" into a heat-insulating pipe with 0.5-cm-thick walls and, after being rolled into a 17-cm-diameter coil, was buried in the sand box at a depth of 26 cm. Figure 5 shows reconstructed test-object radio images for each of the two orthogonal probing-radiation polarizations (Figs. 5a and 5b) and their sum (Fig. 5c).

Figure 6a presents a three-dimensional radio tomogram of the entire explored space, with Fig. 6b showing the graph of the normed integral distribution of inhomogeneities over the range. All the maxima in this figure have correspondences similar to those in Fig. 4.

Analysis of the results shows that using dual-polarization probing scheme greatly improves the contrast of radio images in the radio tomography of metal-containing cables. For fiber-optic cables, the total radio

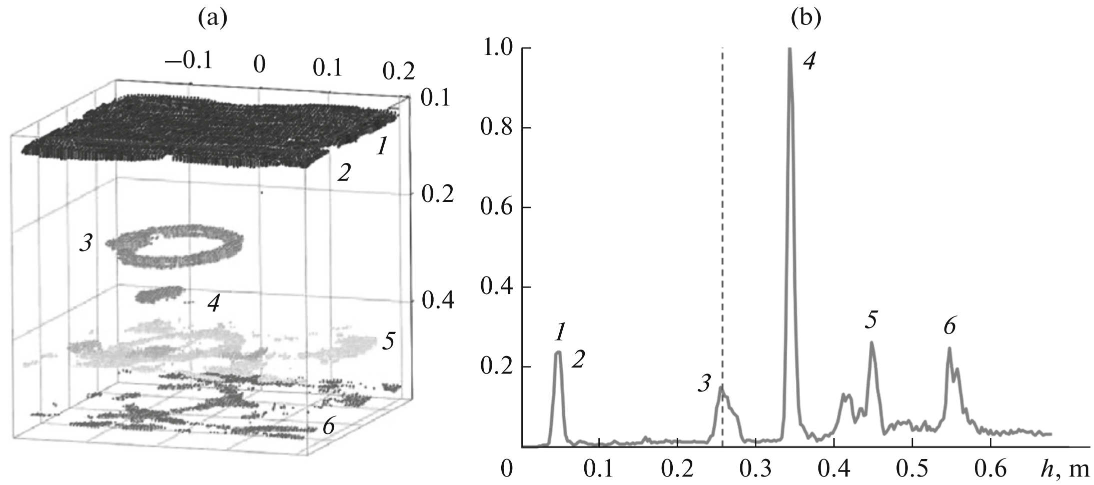

Fig. 6. Three-dimensional radio tomogram of fiber-optic cable (a) and integral distribution of inhomogeneities over range (b).

image possesses a higher contrast ratio, but even single-polarization measurements yield high-quality radio tomograms. Based on the radio images of the cables, the resolving ability of the radio tomograph can be estimated at around 2 cm.

CONCLUSIONS

In this work, the method of tomosynthesis has been experimentally tested for layer-by-layer reconstruction of the radio images of cables with and without metal when probing with two orthogonal polarizations. The radio tomograms of test objects have been obtained with a resolving ability close to the limiting one for the selected probing-radiation frequency band. The achievable resolution at the frequency of 10 GHz is 1.5 cm. Using the example of a “twisted pair” cable, it has been demonstrated that dual-polarization probing significantly increases radio-image contrast ratio.

ACKNOWLEDGMENTS

This work was carried out as part of the State Order #3.2068.2017/4.6 from the RF Ministry of Education and Science.

REFERENCES

1. *Voprosy podpoverkhnostnoi radiolokatsii. Kollektivnaya monografiya* (On the Issues of Subsurface Detection and Ranging: a Collective Monograph), *Grinev*, A.Yu, Ed., Moscow: Radiotekhnika, 2005.
2. Yakubov, V.P., Shipilov, S.E., Sukhanov, D.Ya., and Klokov, A.V., *Radiovolnovaya tomografiya: dostizheniya i perspektivy* (Radio Wave Tomography: Achievements and Prospects), Tomsk: NTL, 2014.
3. Charvat, G., Kempel, L., Rothwell, E., Coleman, C., and Mokole, E., A through-dielectric ultrawideband (UWB) switched-antenna-array radar imaging system, *IEEE Trans. Antennas Propag.,* 2012, vol. 60, no. 11, pp. 5495–5500.
4. Stolt, R.H., Migration by Fourier transform, *Geophysics,* 1978, vol. 43, no. 1, pp. 23– 48.
5. Yakubov, V.P., Shipilov, S.E., and Satarov, R.N., Ultra-wideband sensing behind dielectric barriers, *Russ. J. Phys.,* 2010, vol. 53, no. 9, pp. 887–894.
6. Zhang, W., Hoorfar, A., and Li, L., Through the wall target localization with time reversal method, *Prog. Electromagn. Res.,* 2010, vol. 106, pp. 75–89.

Translated by V. Potapchouck